JOURNAL OF ENZYME INHIBITION AND MEDICINAL CHEMISTRY
2018, VOL. 33, NO. 1, 1212–1224
https://doi.org/10.1080/14756366.2018.1491564

Taylor & Francis
Taylor & Francis Group

RESEARCH PAPER

OPEN ACCESS Check for updates

Donepezil structure-based hybrids as potential multifunctional anti-Alzheimer's drug candidates

Luca Piemontese[a,b], Daniel Tomás[a], Asha Hiremathad[a], Vito Capriati[b], Emanuel Candeias[c], Sandra M. Cardoso[c,d], Sílvia Chaves[a] and M. Amélia Santos[a]

[a]Centro de Química Estrutural, Instituto Superior Técnico, Universidade de Lisboa, Lisbon, Portugal; [b]Dipartimento di Farmacia–Scienze del Farmaco, Università degli Studi di Bari "Aldo Moro", Consortium C.I.N.M.P.I.S, Bari, Italy; [c]CNC–Center for Neuroscience and Cell Biology, University of Coimbra, Coimbra, Portugal; [d]Institute of Molecular and Cell Biology, Faculty of Medicine, University of Coimbra, Coimbra, Portugal

ABSTRACT

A new series of multifunctional hybrids, based on the structure of the donepezil (DNP) drug, have been developed and evaluated as potential anti Alzheimer's disease (AD) agents. The rationale of this study was the conjugation of a benzylpiperidine/benzylpiperazine moiety with derivatives of bioactive heterocyclics (benzimidazole or benzofuran), to mimic the main structure of DNP and to endow the hybrids with additional relevant properties such as inhibition of amyloid beta (Aβ) peptide aggregation, antioxidant activity and metal chelation. Overall, they showed good activity for AChE inhibition (IC_{50}=4.0–30.0 μM) and moderate ability for inhibition of $A\beta_{1-42}$ self-mediated aggregation. The hybrids containing chelating groups showed improvement in the inhibition of Cu-induced $A\beta_{42}$ aggregation and the antioxidant capacity. Moreover, neuroprotective effects of these compounds were evidenced in neuroblastoma cells after $A\beta_{1-42}$ induced toxicity. Structure–activity relationship allowed the identification of some promising compounds and the main determinant structural features for the targeted properties.

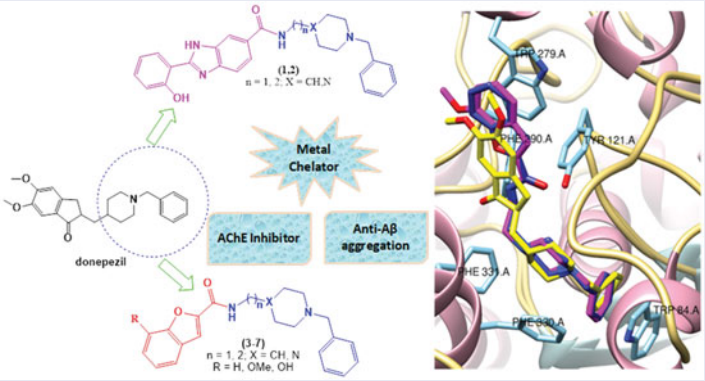

ARTICLE HISTORY
Received 15 May 2018
Revised 16 June 2018
Accepted 17 June 2018

KEYWORDS
Alzheimer's disease; multipotent drugs; donepezil mimetics; AChE inhibitors; anti-Aβ aggregation

1. Introduction

Alzheimer's disease (AD) is a progressive age-dependent neurodegenerative disorder with no cure so far, affecting approximately 47 million individuals worldwide[1].

Although AD pathogenesis is complex and unclear, an increasing number of biological targets have been identified and investigated over the last two decades, most of them related with the main hallmarks of AD patient brains, such as amyloid plaques of amyloid beta (Aβ) peptide aggregates, the tau protein aggregates and also the recovery of the cholinergic deficit by inhibition of acetylcholinesterase (AChE)[2,3]. Other prominent AD targets have been the object of intensive research, under an individual or multiple pharmacophore strategy[4], such as enzymes (beta-secretase and monoamine oxidases)[5], receptors (*N*-metil-D-aspartate (NMDA) and peroxisome proliferator-activated (PPAR)[6]), oxidative stress[7] and biometal dyshomeostasis[8,9]. Interestingly, there has also been a recent interest in exploring the role of natural compounds as drugs or drug coadjuvants in the treatment of AD[10].

Up to now, only five drugs have been approved by the USA Food and Drug Administration (FDA) for use in AD, but they only have palliative effects with temporary symptomatic reliefs. Four of these drugs are AChE inhibitors [e.g. tacrine (no longer in clinical use) donepezil (DNP), rivastigmine, galantamine], while one (memantine) is a NMDA receptor antagonist[1,2]. Therefore, the absence

CONTACT M. Amélia Santos masantos@ist.utl.pt Centro de Química Estrutural, Instituto Superior Técnico, Universidade de Lisboa, Av. Rovisco Pais 1, Lisbon 1049-001, Portugal

Supplemental data for this article can be accessed here.

© 2018 The Author(s). Published by Informa UK Limited, trading as Taylor & Francis Group.
This is an Open Access article distributed under the terms of the Creative Commons Attribution-NonCommercial License (http://creativecommons.org/licenses/by-nc/4.0/), which permits unrestricted non-commercial use, distribution, and reproduction in any medium, provided the original work is properly cited.

of disease-modifying drugs against AD, and the recognised multifactorial origin of this disease, has stimulated an intensive research activity focused on the development of multi-target drugs to address the potential multiple events involved at the onset and/or during the progress of this disease, thereby improving the therapeutic efficacy[4,9,11–15]. Engaged in this drug discovery strategy, a lot of research has been inspired by the structures of AChE inhibitor (AChEi) drugs, such as tacrine, DNP and rivastigmine, which are conjugated or hybridised with other pharmacophoric moieties for hitting other AD targets. Although tacrine has been by far the most explored AChEi for extra-functionalisation or hybridisation[4,13,15–17], hybrids based on the structure of other AChEis, namely DNP, have also been reported[14,18–21].

Pursuing the challenge of developing new multi-target anti-AD drugs, in this article we describe the design, synthesis and biological evaluation of a series of new DNP-like hybrids (see Figure 1), which include DNP biomimetic segments (*N*-benzylpiperidine and *N*-benzylpiperazine) linked to bioactive heterocyclic moieties, namely derivatives of benzimidazole and benzofuran, two scaffolds with recognised importance in medicinal chemistry[22–24], which have also been recently included in the structure of anti-neurodegenerative agents[19,25,26]. Therefore, besides the AChEi activity due to the DNP fragment, these novel hybrids are endowed with potential anti-Aβ aggregation capacity, anti-oxidant activity and metal chelating properties.

The new hybrids are assayed for AChE inhibition, anti-oxidant activity and also anti-amyloidogenic activity by inhibition of $A\beta_{42}$ peptide aggregation in the presence or absence of copper. In addition, the neuroprotective effect of the developed ligands is tested in neuroblastoma cells treated with $A\beta_{42}$ peptide as an AD stress model. Furthermore, molecular simulation studies are performed to aid the molecular design of the compounds based on their binding interactions with the AChE active site, to investigate the structure–activity relationships of the compounds, and also to anticipate their drug-like properties.

2. Results and discussion

2.1 Molecular design and modelling

The design of seven novel multi-target compounds (Figure 1) was based on linking two molecular moieties with potential anti-neurodegenerative properties. Considering that DNP is the current first choice drug for AD treatment, it was our first pharmacophore inspiration, leading to the selection of *N*-benzylpiperidine and its isostere benzylpiperazine[27], to mimic the binding interaction of DNP within the catalytic anionic site (CAS) of AChE[4]. These moieties were hybridised with benzimidazole or benzofuran derivatives, in order to mimic the indanone segment of DNP in its interaction with the peripheral anionic site (PAS) of AChE, and also to provide additional properties to the hybrids, namely antioxidant, anti-$A\beta_{42}$ aggregation and metal chelating activity. Each pair of these main molecular moieties was linked through a 1- or 2-methylene chain.

Since the DNP–AChE binding interactions are described in literature[28], preliminary docking studies have been herein undertaken to see whether most of these interactions could be accomplished by the new series of compounds. DNP is known to present a strong binding with the active site of human acetylcholine esterase *h*AChE, and also of the electric ray (*Torpedo californica*) homologue. In spite of some differences reported for the corresponding inhibitor–enzyme complexes, these enzymes are quite conservative in terms of the main aminoacid residues that are lining the active site gorge[29]. In particular, the binding of DNP with *Tc*AChE includes three distinct interactions: in the bottom of the gorge, the benzyl group establishes a parallel π–π stacking with the indole group of Trp84; in the middle of the gorge, the

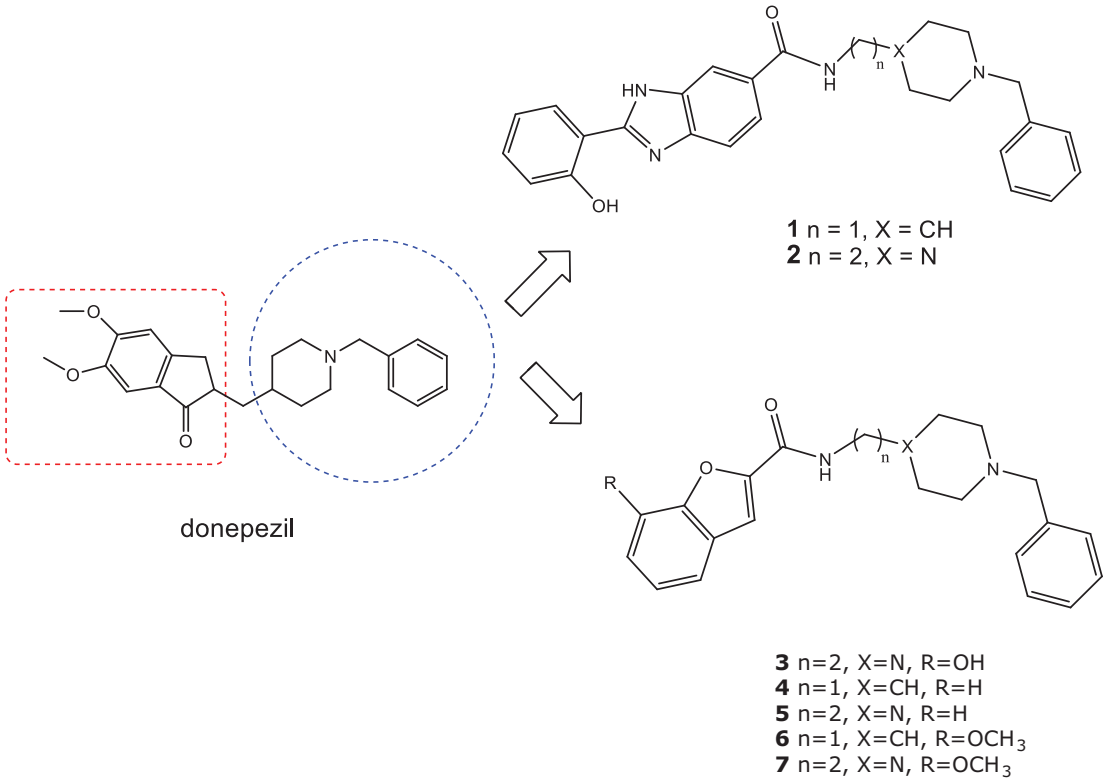

Figure 1. Schematic representation of the design strategy for the novel multi-target mimics of DNP.

charged nitrogen atom can establish a cation–π binding interaction with the phenyl group of Phe330; at the entrance of the gorge, the indanone ring interacts through π–π stacking with the peripheral anionic residue Trp279. In fact, the docking simulations with our compounds showed they could get a similar accommodation in the gorge of the enzyme, namely concerning the interaction of the DNP-like moieties (benzylpiperidine or benzylpiperazine) with the aminoacid residues of CAS. At the same time, the benzimidazole or benzofuran moieties are engaged in the interactions with PAS. These planar heterocyclic rings also seem to allow a π–π interaction with the indole group from Trp279, but apparently with less favourable orientation than with DNP.

Of note, as compared with the original ligand (DNP), compounds **1** and **2** show an excellent superimposition in CAS, (Figure 2a), while in the PAS some deviation appears, potentially because the hydroxyphenylbenzimidazole (BIM) moiety has a longer size than that of the DNP indanone group.

However, the presence of an extra methylene group in the linker of compound **2** may apparently lead to a better accommodation of the benzimidazole ring, which appears at a closer distance to the indole ring of Trp279 than compound **1**. Comparison among the benzofuran series (compounds **3–7**) did not evidence much difference. Although the methoxy group of compounds **6–7** does not seem to present by itself any extra interaction within the *Tc*AChE active site (Figure 2b), it may work similarly to the methoxy groups of the DNP indanone, which seems to be involved in the formation of water-mediated hydrogen bonds with the enzyme, according to reported crystal structure of *Tc*AChE or *h*AChE with DNP[26].

2.2 Chemistry

Compounds **1–7** were synthesised according to Schemes 1–3.

The molecular fragments **8–11** were prepared according to standard procedures (Scheme 1). Intermediate **8** was synthesised by a Mannich reaction between 3,4-diamino benzoic acid and salicylaldehyde followed by cyclisation, aided by the reducing agent sodium metabisulfite[30]. Intermediates **9** and **10** were obtained from the reaction with ethyl bromoacetate and the suitable salicylaldehyde, followed by hydrolysis under basic conditions. Compound **11** was obtained starting from **10**, by demethylation in the presence of BCl_3 and tetrabutylammonium iodide[31].

Intermediates **12** and **13** were prepared according to the procedure outlined in Scheme 2. *N*-benzylation of the cyclic amine involved a preliminary orthogonal protection of the primary alkylamine side group as a phthalimide by reaction with phthalic anhydride at 160 °C without solvent[32]. The subsequent *N*-benzylation involved a reaction with benzyl chloride under basic conditions. Finally, the title compounds were obtained as free amines through deprotection of the corresponding phthalimide with hydrazine hydrate in ethanol under reflux[33].

The final ligands **1–7** were obtained by coupling reactions between the primary amine group of the benzyl–piperidine/piperazine intermediates and the carboxylic groups of the benzimidazole/benzofuran moieties *via* amide bond formation. Two different amino-carboxylic condensation methods were used in these syntheses, as described in Scheme 3A and B. In particular, compounds **1–3** were obtained by the reaction of **12** or **13** with **8** or **11** in presence of dicyclohexylcarbodiimide (DCC) and *N*-hydroxysuccinimide, while compounds **4–7** were synthesised using propylphosphonic anhydride (T3P) as the coupling reagent, in the presence of *N*-methylmorpholine (NMM) at room temperature.[16] Although the use of the coupling agent T3P has advantages over DCC, namely in terms of reaction working-up, it failed for the phenol containing carboxylic intermediates, presumably due to the reactivity of the phenol group with T3P.

2.3. Biological activity

2.3.1. AChE inhibition

All the tested compounds were assayed for AChE inhibition, following a reported method[31], and showed a good activity, in low

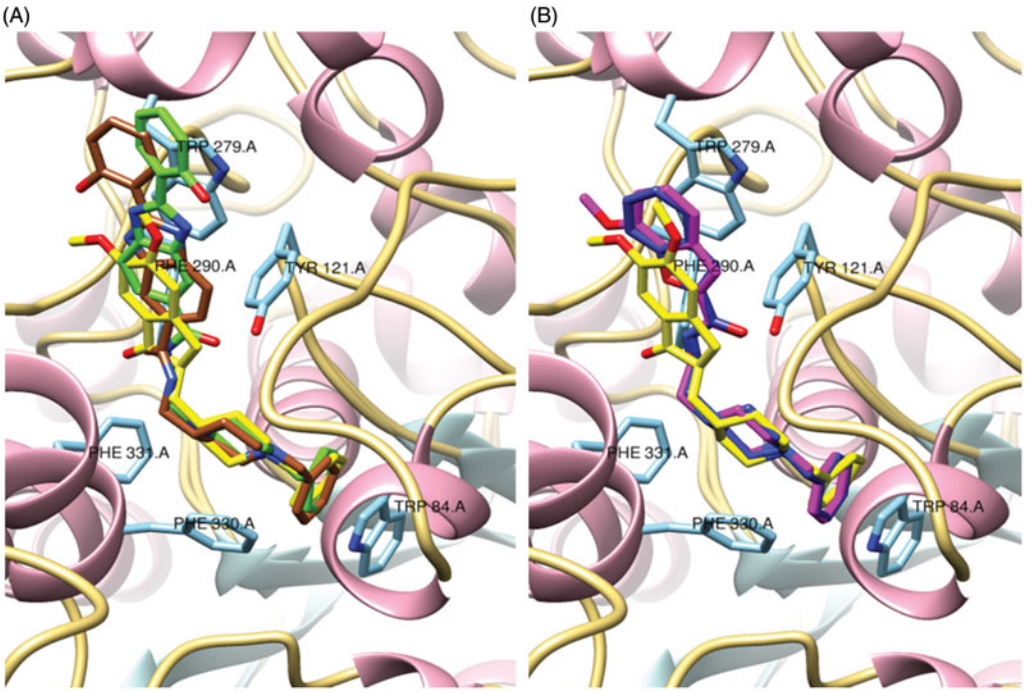

Figure 2. Superposition of a selection of ligands in study and the original ligand (DNP), from PDB code 1EVE, inside the *Tc*AChE active site: (a) DNP (yellow), compound **1** (brown), compound **2** (green); (b) DNP (yellow), compound **5** (blue), compound **7** (magenta).

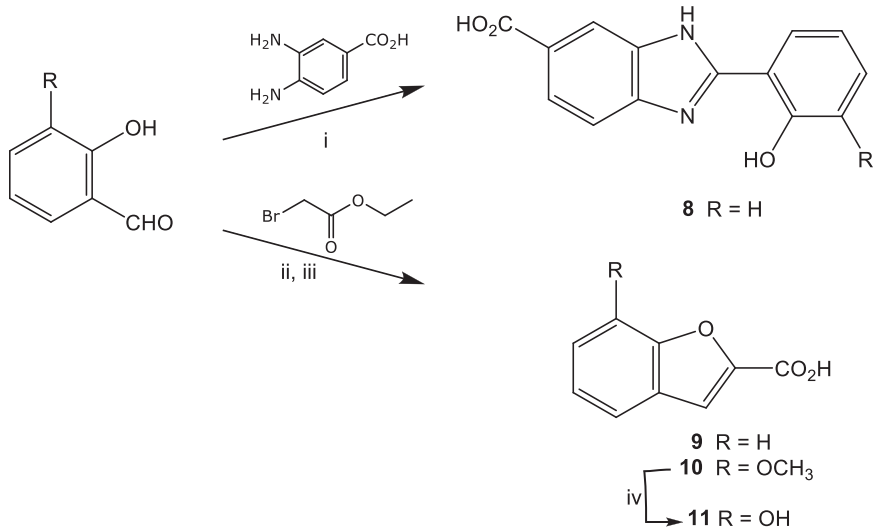

Scheme 1. Reagents and conditions: (i) $Na_2S_2O_5$, dimethylacetamide, 100 °C, 12 h. (ii) K_2CO_3, DMF, reflux, 6 h; (iii) 2 N NaOH, THF, RT, overnight; (iv) BCl_3 (1 M in anhydrous CH_2Cl_2), TBAI, anhydrous CH_2Cl_2, 0 °C, then RT, overnight.

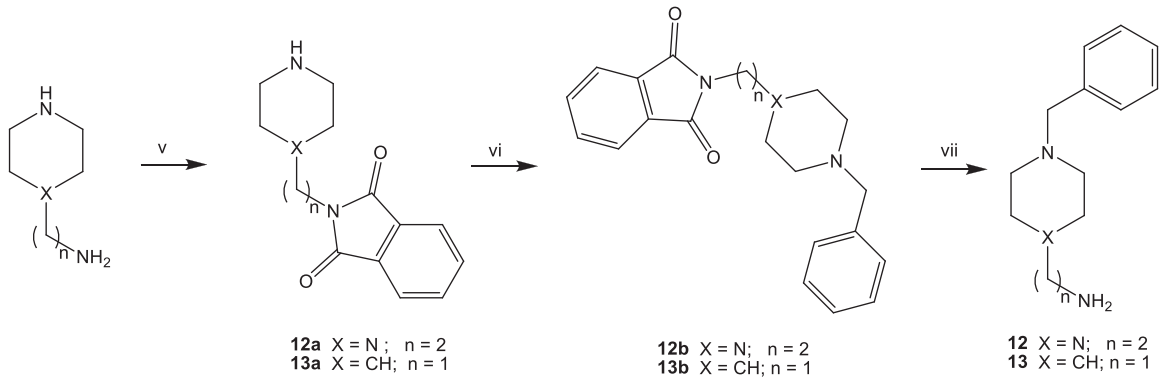

Scheme 2. Reagents and conditions: (v) phthalic anhydride, 160 °C, 4 h; (vi) benzyl chloride, K_2CO_3, triethylamine, acetonitrile, 50 °C, 3 h; (vii) N_2H_4 xH_2O, absolute ethanol, reflux, 3 h, then RT, overnight.

micromolar range (IC_{50}=4.0–30.0 μM, Table 1). These values are higher than those of DNP or tacrine, but within the purposes of the projected drug strategy. Generally it can be assumed that the great advantages of the multi-target drugs in multifactorial complex diseases can overcome the disadvantage of losing some activity relative to a specific property of a single-target drug.

All the compounds present quite good activity (IC_{50} in low micromolar range) as supported by the docking simulations (Figure 2 and Figure S2), showing a similar accommodation and interactions within the CAS, analogously to those of DNP. In particular, they share a π–stacking interaction (between the phenyl of the benzyl–piperidine/piperazine moiety and the aromatic residue Trp84) and also a cation–π interaction between the protonated nitrogen atom of benzylamine and the Phe330. Generally, except compound **7**, the hybrids with the BIM motif (**1** and **2**) showed a slightly higher AChE inhibition, than the corresponding benzofuran derivatives, which should be due to more favourable interactions within the PAS. Regarding the benzofuran-containing compounds, those with the piperazine ring (**3**, **5** and **7**) showed better inhibition values than the piperidinic analogues (**4** and **6**), although that effect was not evidenced for benzimidazole derivatives (**1** and **2**). Therefore, the extra methylene group in the linker of the piperazinic derivatives may result in a slight detrimental effect in the BIM hybrids, apparently due to weaker binding interactions in the PAS, namely the π–stacking interaction with Trp279 (Figure 2 and Figure S2). However, according to the docking simulation, that effect may not be so relevant for the benzofuran derivatives due to the smaller size of this moiety as compared with the BIM moieties. On the other hand, the second nitrogen atom of the piperazine ring may also favour some positive interactions within the CAS. Compound **7** (IC_{50}=4.0 ± 0.4 μM) showed the best AChE inhibitory capacity, similar to compound **1** (IC_{50}=4.2 ± 0.8 μM) and **2** (IC_{50}=6.9 ± 0.7 μM). This may also be due to some role of the methoxy group, which similarly to DNP, may also establish some extra-interaction or promote of a better orientation of the heterocyclic ring inside the PAS as suggested by the docking results (Figure S2b).

2.3.2. Inhibition of self-mediated and Cu(II)-induced $A\beta_{1-42}$ aggregation

The ability of the studied compounds to inhibit Aβ self-aggregation was assessed based on the change of the fluorescence emission of thioflavin T (ThT) associated to fibril binding[16]. Analysis of the results presented in Table 1 shows a moderate inhibition of $A\beta_{1-42}$ aggregation. In general, the hybrids with the benzimidazole moiety (**1–2**) proved to be more active than those with the benzofuran counterparts (**3–7**), with the exception of compounds **3** and **6**, whose inhibition values are in the same range of the benzimidazole derivatives. On the other hand, the piperidine series seems to be more effective than the piperazine one, while the methoxy substituent on the benzofuran ring (compounds **6** and

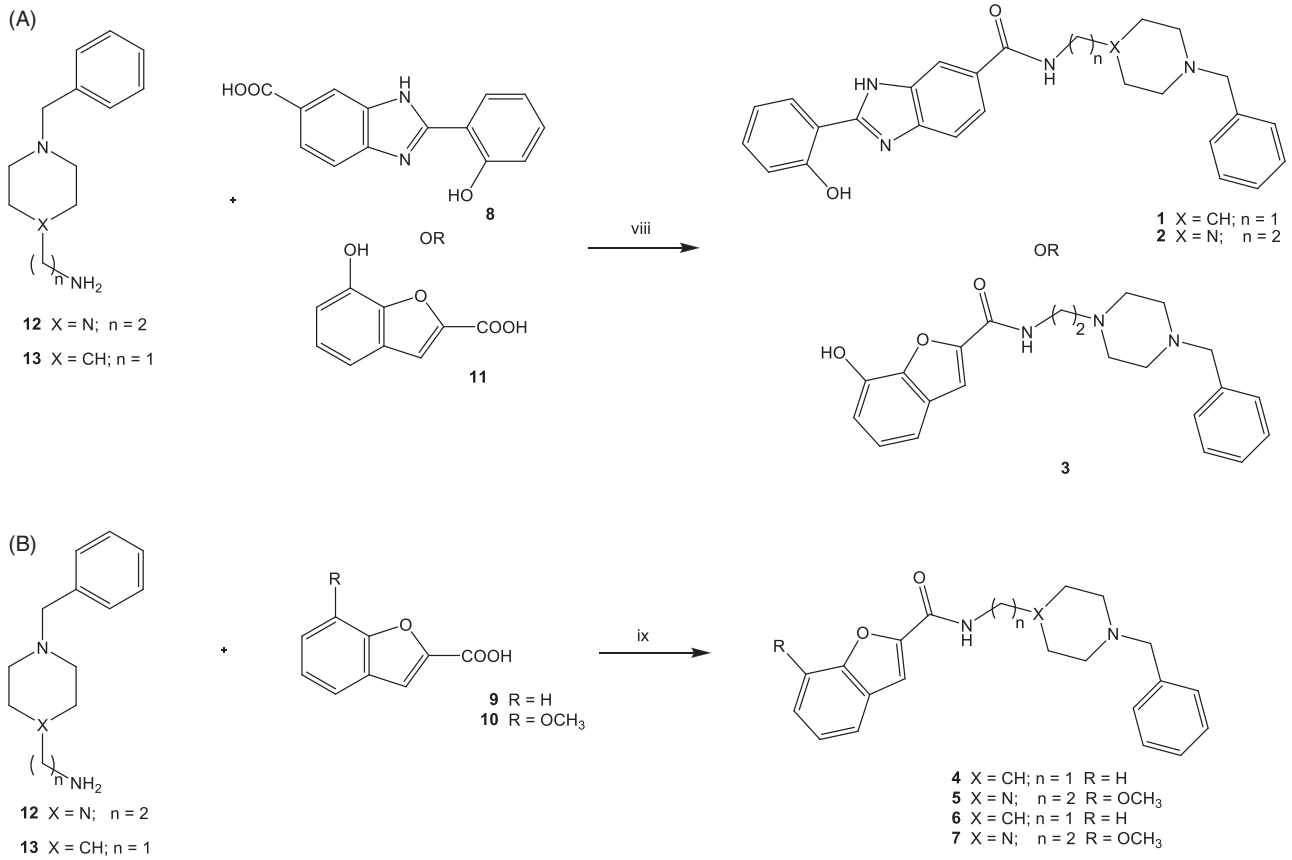

Scheme 3. Reagents and conditions: (a) (viii) DCC, *N*-hydroxysuccinimide, dry DMF, RT, 40 h. (b) (ix) T3P, NMM, dry CH_2Cl_2, RT, overnight.

Table 1. Biological properties of the hybrids: inhibition of AChE (Electric eel) and self-mediated $A\beta_{1-42}$ aggregation.

Compound	AChE inhib.[a] IC_{50} ±SD (μM)	$A\beta_{1-42}$ aggregation inhibit. (%)[b]
1	4.2 ± 0.8	36.3
2	6.9 ± 0.6	25.3
3	20.0 ± 0.8	27.3
4	30.0 ± 0.9	14.5
5	18.5 ± 0.9	14.4
6	19.9 ± 3.0	26.9
7	4.0 ± 0.4	19.0
Tacrine	0.15 ± 0.02	21.2c
DNP	0.025d	–

[a]The values are mean of five independent experiments ± SD.
[b]Inhibition of self-mediated $A\beta_{1-42}$ aggregation (in %) by thioflavin-T fluorescence method; measurements were carried out in presence of an inhibitor (80 μM) for 40 μM $A\beta_{1-42}$ and the values are mean of two independent measurements in duplicate (SEM <10%).
[c]Ref. 19
[d]Ref. 4.

7) seems to improve the activity, as compared with the non-substituted analogues (**4** and **5**). The inhibition of Aβ aggregation by the planar heterocyclic compounds may be associated with the disruption of the conformation in β-sheets, as previously suggested[16].

In order to support these results, the best inhibitor (compound **1**) was tested with an independent imaging technique, by transmission electron microscopy (TEM), so as to visualise the differences in $A\beta_{1-42}$ aggregation in the presence and in the absence of the inhibitor. Although Aβ aggregates are still evident (Figure 3a and b), in the presence of the inhibitor, they became quite sparse. This behaviour was expected, considering the moderate percentage of Aβ aggregation inhibition (ca. 36%) found for compound **1**. Regarding the morphology of the aggregates, in the absence of compound **1** they appeared more dense and amorphous, while in its presence some elongated singular branches were observed possibly due to ligand intercalation between β-sheets of Aβ fibrils. Compound **2** was already assayed by TEM and a reduction of Aβ aggregates was also observed, thereby proving the anti-Aβ aggregation ability of this compound[34].

Due to the known role of metals, in particular copper(II) in Aβ aggregation and amyloid plaque formation[8,35], compounds **2** and **3** were also studied for their ability to inhibit the aggregation in the presence of copper(II). This option was also based on the fact that preliminary chelation studies with compound **2** showed good ability for the complexation of copper(II) (pCu =11.4 at physiological pH, C_L/C_M=10, C_M=1 μM)[34], whereas the hydroxyl–benzofuran moiety of tacrine-(hydroxyl–benzofuran) hybrids proved also to be a good Fe(III) and Cu(II) chelator[36]. The improved capacities of compounds **2** and **3** to inhibit Aβ aggregation in the presence of copper(II) (37.7% and 35.5%), as compared with the corresponding inhibition of the self-mediated aggregation (25.3% and 27.3%), suggests that the copper(II) chelation may interfere with the formation of Aβ aggregates by competition with the amyloid peptide for the metal ion, which is necessary for the stability of the structure, as already reported in our recent past papers[16,31]. The TEM images enclosed in Figure 3c and d confirm the apparent role of Cu(II) chelation in the reduction of Aβ aggregates by compound **1**, as already found for compound **2**[34].

2.3.3. Antioxidant activity

Among the studied ligands, only the compounds with benzimidazole motif were tested for the antioxidant activity (radical

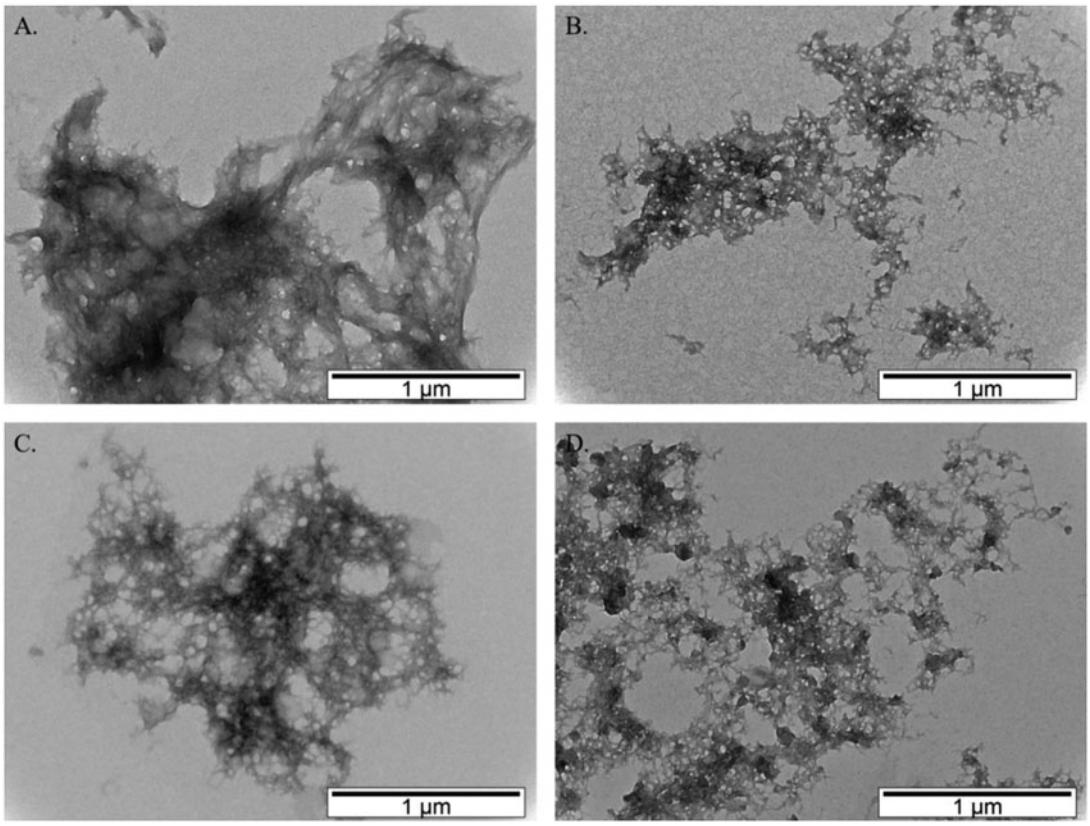

Figure 3. TEM images of Aβ self-aggregation inhibition experiments of compound **1**: (a) absence of compound **1** and absence of copper; (b) presence of compound **1** and absence of copper; (c) absence of compound **1** and presence of copper; (d) presence of compound **1** and presence of copper.

Table 2. Pharmacokinetic properties as predicted *in silico* by software QikProp v.2.5[40].

Comp.	MW (Da)	clog *P*	log BB	Caco-permeability (nm/s)	CNS	Violations of Lipinski's rule
1	440.554	4.386	−0.730	194	–	0
2	455.558	2.587	−0.097	48	+/−	0
3	379.485	2.453	−0.243	56	+	0
4	348.444	3.690	0.077	575	+	0
5	363.458	3.153	0.547	243	++	0
6	378.478	4.371	0.127	905	+	0
7	393.485	2.879	0.132	101	+	0

scavenging capacity), based on their interaction with the 2,2-diphenyl-1-picrylhydrazyl (DPPH) free radical[37]. Compound **2** showed moderate activity, with EC_{50} in high-micromolar range (594 ± 4 μM). Compound **1** should have similar activity, but solubility problems under the used experimental conditions, precluded its evaluation. Regarding the benzofuran derivatives, only for compound **3,** containing a hydroxyl–benzofuran moiety, it is expected a radical scavenging activity in the same range, similarly to other (hydroxyl–benzofuran)–tacrine hybrids (EC_{50}=396–480 μM; EC_{50} (tacrine >1000 μM)[31]. This anti-oxidant activity is attributed to the phenolic group which is known to have an important role in the scavenging of reactive oxygen species by H-atom abstracting reactions[38]. The values obtained herein, compared with those typical of the reference polyphenolic antioxidant, Trolox (EC_{50}=15 μM)[39], using the same experimental method, indicates a quite moderate activity for the studied compounds.

2.3.4. Predictive pharmacokinetic properties

In an effort to assess the drug-likeness of the novel compounds and their potential to penetrate important membranes such as the blood–brain barrier (BBB), some indicators of their pharmacokinetic profiles were predicted using QikProp program, v. 2.5[40]. Parameters such as the calculated octanol–water partition coefficient (clog *P*), the ability to cross the BBB (log BB), the capacity to be absorbed through the intestinal tract to the blood (Caco-2 cell permeability), the activity on the central neuronal system (CNS) and the verification of Lipinski's rule of five[41] were analysed to evaluate their drug-likeness as potential orally active anti-AD agents.

Analysis of Table 2, containing the main calculated pharmacokinetic descriptors, shows that all compounds are free from violations of Lipinski's rule. This suggests the appropriateness for oral administration. In particular, all the compounds synthesised have molecular weight below 500 and clog *P* in the range (2.6–4.4), while the Caco-permeability values appear in a wide range, which can be considered moderate to good (higher than 500 nm/s) for compounds **4** and **6**. Particularly important for our studies is the predicted log BB value, which gives information about the distribution of the compound between the blood and the brain. All the compounds show values within the range defined by the software [−3 (excellent) to 1.2 (bad)][40]. Concerning the predicted activity in the CNS, compound **5**, which has the highest log BB value (0.547), presents the best activity (++), while compound **1,** with the lowest log BB (−0.730), presents the lowest activity (–). In

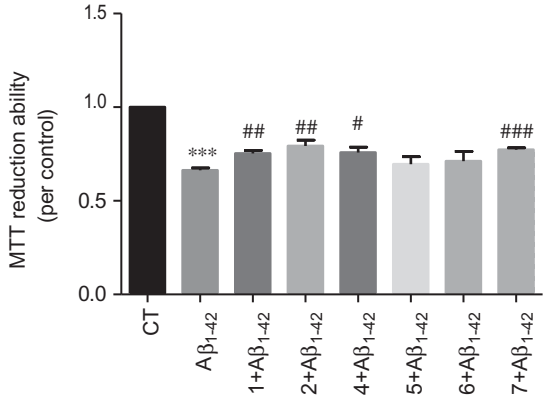

Figure 4. Effect of the selected hybrids on Aβ42-induced toxicity on SH-SY5Y cells. Cells were treated with Aβ42 peptide (1 μM), for 24 h after treatment for 1 h in the absence or the presence of the compounds. Evaluation of cell proliferation was performed by using MTT reduction assay. Results are expressed as the percentage of SH-SY5Y untreated cells, with the mean ± SEM derived from three different experiments. $^{***}p < 0.001$, significantly different when compared with SH-SY5Y untreated cells; $^{\#}p < 0.05$, $^{\#\#}p < 0.01$ and $^{\#\#\#}p < 0.001$, significantly different when compared with Aβ42 treated SH-SY5Y cells. (Abeta-1 μM; compounds: **1**–2,5 μM; **2**–5 μM; **4, 5** and **7**–30 μM; **6**–20 μM).

summary, these predictions indicate that, generally, these hybrids present good BBB permeability (log BB), therefore becoming eligible as drug candidates for oral administration.

2.3.5 Cell viability

The potential therapeutic effect of the new ligand hybrids was evaluated based on the structure of DNP using SH-SY5Y cells treated with $A\beta_{1-42}$ peptides. For each compound, a dose–response curve was performed to select a nontoxic concentration in order to analyse the neuroprotective effect (Figure S1). While the aetiology of AD remains largely unclear, recent evidences indicate that an increased formation of oligomeric Aβ species is involved in the neurodegenerative process of AD[3]. It was observed that Aβ induced a decrease in cell viability and, interestingly, compounds **1**, **2**, **4** and **7** prevented partially from Aβ-induced cell toxicity (Figure 4).

Indeed, compounds **1** and **2** also showed high inhibition of AChE and Aβ aggregation. In addition, compound **2** also presents the more relevant antioxidant capacity.

3. Conclusion

Over the few last years, the conjugation of two or more different active moieties in only one molecule has been accepted as an important strategy in the design of new drugs able to face multifactorial diseases such as AD. Following this approach, seven new multi-target ligands were designed, synthesised and tested for their activity as inhibitors of AChE and Aβ aggregation (self- and Cu(II)-mediated) as well as for their anti-oxidant capacity. The hybrid structures include a moiety derived from a commercial anti-AD drug, DNP, connected by a 1–2 methylene bridge with a substituted planar heterocyclic structure. As hypothesized, the AChE inhibitory activity was preserved, with IC_{50} in low-μM range but higher than that of the parent drug DNP, due to the weak binding of the benzylpiperazine or *N*-benzylpiperidine portion with the CAS of AChE. Insertion of a heterocyclic planar group led to a moderate inhibition of Aβ self aggregation, while the inhibition of the Cu^{2+}-induced Aβ aggregation was particularly enhanced for compounds with metal chelation capacity. Some compounds (**1**, **2**, **4** and **7**) showed neuroprotective roles by preventing the Aβ-induced cell toxicity. A moderate anti-oxidant activity is also associated to the phenol-containing hybrids. The calculated pharmacokinetic parameters indicate a good profile for the main molecular descriptors with no violation of Lipinski's rules. Summarising, the comparative analysis of the obtained biological data for the studied compounds shows that conjugation of these different scaffolds in a single molecule provided a basis for the development of potential multi-target drug candidates for the treatment of the multifactorial AD pathology.

4. Experimental section

4.1 Materials and methods

Reagents and solvents were purchased from common suppliers and were used as delivered. Whenever necessary, solvents were dried in our laboratory according to the standard procedures[42].

Reactions were monitored by pre-coated thin layer chromatography (TLC) plates (Merck silica gel 60_{F254}). Silica gel60 (0.063–0.200 mm) was used for column chromatography. Melting points were measured with a Leica Galen III hot stage apparatus and are uncorrected. The ^{1}H and ^{13}C NMR spectra were recorded on Bruker AVANCE III-400 (400 MHz, 100.5 MHz) and Bruker AVANCE III (300 MHz, 75.5 MHz) NMR spectrometers, at 25 °C using residual peaks of solvents as an internal standard. The chemical shift values are on a δ scale.

The antioxidant and AChE inhibitory activities were determined by using a Perkin Elmer Lambda 35 spectrophotometer equipped with a temperature programmer PTP 1 + 1 Peltier System, using thermostated ($T = 25.0 \pm 0.1$ °C) 1 cm path length cells.

Amyloid β peptide (1–42) ($A\beta_{1-42}$) was purchased from GeneCust as a lyophilised powder and stored at −20 °C. The ThT fluorescence was measured using a spectrofluorimeter Varian Cary Eclipse at 446 nm (excitation) and 485 nm (emission). Transmission electron microscopy (TEM) images were taken by a Hitachi H8100 TEM with a LaB6 filament (200 kV, 10000–20000× magnification) in MicroLab/IST.

Electrospray ionisation-mass spectrometry (ESI-MS) experiments were carried out on a LCQ Fleet mass spectrometer operated in the ESI positive and negative ion modes (Thermo Scientific).

HPLC-HRMS analyses were performed with a benchtop single-stage mass spectrometer (Exactive) equipped with a heated electrospray ion source (HESI II) (Thermo Fisher Scientific, Bremen, Germany), coupled to an Accela HPLC system (Thermo Fisher Scientific, San Jose, CA, USA), using Gemini C18 column (150 mm ×2 mm, 5-μm particles; Phenomenex, Torrance, CA, USA), preceded by a Gemini C18 guard column (4 mm × 2 mm, 5-μm particles). The mobile phase was a gradient of water/methanol from 10 to 40% MeOH in 3 min, then to 48% MeOH in 12 min, to 90% MeOH in 15 min and then maintained at 90% MeOH for 8 min (total run 38 min). The column was then brought to 10% MeOH in 1 min and left to equilibrate for 7 min before to the next run.

4.2 Molecular modelling studies

The docking calculations were performed following a procedure identical to that previously reported[43]. The X-ray crystallographic structure of *T. californica* AChE (*Tc*AChE) complexed with the enzyme inhibitor DNP was taken from RCSB Protein Data Bank (PDB entry 1EVE), in order to be used as a receptor model in the docking simulations. The original complex structure model was treated using Maestro v. 9.3[44] to remove the original ligand, solvent and co-crystallisation molecules as well as to add hydrogen

atoms. This program was also used to design the ligand structures, which were submitted to random conformational search (RCS) of 1000 cycles and 2500 optimisation steps with the program Ghemical v 2.0[45,46]. The ligands were docked into the AChE structure, using GOLD v. 5.1[47] with the default parameters of GOLD (except "allow early termination" option) and the Astex Statistical Potential (ASP) scoring function. The zone of interest was defined as the residues within 10 Å from the original position of the ligand in the crystal structure.

4.3 Synthetic procedures

4.3.1. 2-(2-Hydroxyphenyl)-1H-benzo[d]imidazole-5-carboxylic acid (8)

3,4-Diaminonbenzoic acid (152 mg, 1 eq) and $Na_2S_2O_5$ (266 mg, 1.4 eq) were added to a solution of salicylaldehyde (122 mg, 1 eq) in *N*,*N*-dimethylacetamide. The mixture was heated at 100 °C for 12 h and then cooled to room temperature. Then, the solution was diluted in ethyl acetate, dried over anhydrous sodium sulphate and concentrated under reduced pressure. The product was dried under vacuum, affording a pale brown solid. Yield = 67%, m.p. >300 °C. 1H NMR (400 MHz, DMSO-d_6) δ: 7.02–7.08 (dd, $J = 15.6$, 7.1 Hz, 2H, H-10 & H-11), 7.41 (t, $J = 7.4$ Hz, 1H, BIM-H-9), 7.73 (d, $J = 7.7$ Hz, 1H, BIM-H-5), 7.91 (d, $J = 7.9$ Hz, 1H, BIM-H-4), 8.11 (d, $J = 8.1$ Hz, 1H, BIM-H-3), 8.24 (s, 1H, BIM-H-2); MS-ESI (*m/z*): 253 $(M-1)^+$, 254 $(M)^+$, 255 $(M+1)^+$.

4.3.2. General method for the synthesis of benzofuran-2-carboxylic acid derivatives (9 and 10)

To a solution of the salicylaldehyde derivative (1 eq) and anhydrous K_2CO_3 (276 mg, 2 eq) in DMF, ethyl chloroacetate (135 mg, 1.1 eq) was added. The mixture was heated at 110 °C for 1.5 h. Then, the temperature of the reaction mixture was increased to 150 °C for 4 h, and reaction was monitored by TLC. After consumption of starting material, water was added to the mixture, which was left under reflux for more 1.5 h. The reaction mixture was then cooled to RT and poured into crushed ice. The basic aqueous solution was acidified with HCl to give the final product as a yellow coloured precipitate.

4.3.3. Benzofuran-2-carboxylic acid (9)

Starting from salicylaldehyde (122 mg), yield 85%, m.p. 193–195 °C; ^{1}H NMR (300 MHz, DMSO-d_6), δ (ppm): 7.35 (t, 1H, $J = 7.4$ Hz, O–C–C–CHC*H*), 7.50 (t, 1H, $J = 7.5$ Hz, O-C-CHC*H*), 7.66–7.70 (m, 2H, O-C-C*H*, COOH-C-C*H*), 7.79 (d, 1H, $J = 7.8$ Hz, O-C-C-C*H*); *m/z* (ESI-MS): 163 $(M+H)^+$.

4.3.4. 7-Metoxy-benzofuran-2-carboxylic acid (10)

Starting from *ortho*-vanillin (152 mg), yield 78%, m.p. 221–223 °C; ^{1}H NMR (300 MHz, DMSO-d_6), δ (ppm): 3.95 (s, 3H, OCH_3), 7.08 (d, 1H, $J = 7.1$ Hz, OCH_3–C–C*H*), 7.22–7.33 (m, 2H, O–C–C–C*H*, O–C–C–CH–C*H*), 7.63 (s, 1H, COOH–C–C*H*); *m/z* (ESI-MS): 193 $(M+H)^+$.

4.3.5. 7-Hydroxybenzofuran-2-carboxylic acid (11)

BCl_3 (585 mg, 5 eq) in anhydrous DCM (5 ml) was added dropwise at −78 °C to a solution of 7-methoxybenzofuran-2-carboxylic acid (192 mg, 1 eq) and tetrabutylammonium iodide (1.11 g, 3 eq) in dry DCM under nitrogen atmosphere. The mixture was stirred overnight at RT. Then, the solution was poured into ice and DCM was concentrated under reduced pressure. The aqueous phase was extracted with ethyl acetate (3 times), washed with brine (3 times), dried over anhydrous Na_2SO_4, filtered and concentrated under reduced pressure, affording a brown–pale solid. Yield = 67.4%. ^{1}H NMR (300 MHz, DMSO-d_6), δ (ppm): 6.88–6.90 (dd, 1H, $J = 7.5$, 1.1 Hz, *aromatic*), 7.09–7.25 (m, 2H, *aromatics*), 7.59 (s, 1H, *aromatic*), 10.30 (s, 1H, O*H*); *m/z* (ESI-MS): 179 $(M+H)^+$.

4.3.6. General process for synthesis of the intermediates 12a and 13a

Phthalic anhydride (powder, 148 mg, 1 eq) and 1-(2-aminoethyl)-piperazine or 4-(aminomethyl)piperidine (1 eq) were heated at 160 °C for 4 h. The resulting dark brown solid (1 eq) was mixed with K_2CO_3 (414 mg, 3 eq), triethylamine (153 mg, 1.5 eq) and benzyl chloride (290 mg, 3 eq) and heated at 50 °C in acetonitrile for 3 h. Then, the mixture was cooled at RT, added to water and extracted with ethyl acetate (3 times). The organic layers were collected, dried over anhydrous Na_2SO_4, and concentrated under reduced pressure. The crude was purified by chromatography column (eluent: DCM/MeOH/NH_4OH 92:8:0.1), to give the pure products as light yellow solids.

4.3.7. 2-(2-(4-Benzylpiperazin-1-yl)ethyl)isoindoline-1,3-dione.(12a)

Starting from 1-(2-aminoethyl)-piperazine (129 mg), yield =64.4%. ^{1}H NMR (400 MHz, $CDCl_3$), δ (ppm): 2.39–2.52 (m, 8H, *piperazine*), 2.60 (t, 2H, $J = 6.7$ Hz, phthalimide-CH_2CH_2N), 3.44 (s, 2H, NCH_2Ph) 3.78 (t, 2H, $J = 6.7$ Hz, phtalimide–CH_2CH_2N), 7.19–7.27 (m, 5H, aromatics, *Ph*–CH_2), 7.67–7.69 and 7.80–7.82 (m, 4H, *phtalimide*); *m/z* (ESI-MS): 350 $(M+H)^+$.

4.3.8. 2-((1-Benzylpiperidin-4-yl)methyl)isoindoline-1,3-dione (13a)

Starting from 4-(aminomethyl)piperidine (114 mg), yield =34%. ^{1}H NMR (300 MHz, DMSO-d_6), δ (ppm):1.07–1.15, 1.58–1.76, and 3.44–3.50 (m, 9H, *piperidine*), 2.73 (d, 2H, NCH_2CH) 3.41 (s, 2H, NCH_2Ph), 7.15–7.40 (m, 5H, aromatics, *Ph*–CH_2), 7.79–7.91 (m, 4H, *phthalimide*). ESI-MS (positive, *m/z*): 335 $(M+1)$.

4.3.9. General method for the synthesis of compounds 12 and 13

2-(2-(4-Benzylpiperazin-1-yl)ethyl)isoindoline-1,3-dione (**12a**) or 2-((1-benzylpiperidin-4-yl)methyl)isoindoline-1,3-dione (**12b**) (1 eq) and hydrazine mono hydrate (300 mg, 6 eq) were dissolved in absolute EtOH and stirred for 3 h under reflux and overnight at RT. The reaction mixture was then filtered and concentrated under reduced pressure. The residue was dissolved in ethyl acetate, washed with brine (3 times), dried over anhydrous Na_2SO_4, and concentrated under reduced pressure to obtain a yellow–orange oil, purified through column chromatography (eluent: DCM/MeOH/NH_4OH 92:8:0.1) affording the pure product as a yellow oil.

4.3.10. 2-(4-Benzyl-1-piperazinyl)ethanamine (12)

Starting from 2-(2-(4-benzylpiperazin-1-yl)ethyl)isoindoline-1,3-dione (350 mg, **12a**), yield 99%. ^{1}H NMR (400 MHz, $CDCl_3$), δ (ppm): 2.35–2.43 (m, 10H, *piperazine*, NH_2–CH_2CH_2N), 2.73 (t, 2H, $J = 6.1$ Hz, NH_2–CH_2CH_2N), 3.46 (s, 2H, NCH_2Ph), 7.18–7.27 (m, 5H, aromatics, *Ph*–CH_2); *m/z* (ESI-MS): 220 $(M+H)^+$.

4.3.11. (1-benzylpiperidin-4-yl)methanamine (13)

Starting from 2-((1-benzylpiperidin-4-yl)methyl)isoindoline-1,3-dione (335 mg, **13a**), yield 37%. ^{1}H NMR (300 MHz, DMSO-d$_6$), δ (ppm): 1.00–1.23, 1.61–1.65, 1.82–1.89 and 2.37–2.39 (m, 9H, *piperidine*), 2,77 (d, 2H, $J = 11.5$ Hz, NCH_2CH) 3.41 (s, 2H, NCH_2Ph), 7.20–7.33 (m, 5H, aromatics, *Ph*–CH$_2$); *m/z* (ESI-MS): 205 $(M + H)^+$.

4.3.12. General method for the synthesis of compounds 1–3 (method a)

To a solution of the carboxylic acid derivatives, 2-(2-hydroxyphenyl)-1H-benzo[d]imidazole-5-carboxylic acid (**8**) or 7-hydroxybenzofuran-2-carboxylic acid (**11**) (1 eq), and the amine derivatives, (1-benzylpiperidin-4-yl)methanamine (**13**) or 2-(4-benzyl-1-piperazinyl)ethanamine (**12**), (1 eq) in dry DMF, was added *N*-hydroxysuccinimide (115 mg, 1 eq) and DCC (206 mg, 1 eq) and the reaction mixture was left stirring for 40 h at RT. Then, the obtained white precipitate was filtered off and the liquid phase was diluted with ethyl acetate and washed with brine (3 times), dried over anhydrous Na_2SO_4, concentrated under reduced pressure, and purified through column chromatography affording a solid.

4.3.13. N-((1-benzylpiperidin-4-yl)methyl)-2-(2-hydroxyphenyl)-1H-benzo[d]imidazole-5-carboxamide (1)

Starting from 2-(2-hydroxyphenyl)-1H-benzo[d]imidazole-5-carboxylic acid (**8**) (254 mg) and (1-benzylpiperidin-4-yl)methanamine (**13**), (204 mg) eluent: DCM/MeOH 95:5, then 100% ethyl acetate. The title compound was obtained as a yellow solid, yield =71%; m.p.=265–267 °C. ^{1}H NMR (300 MHz, DMSO-d$_6$), δ (ppm): 1.18–1.23 and 1.58–1.93 (m, 9H, *piperidine*), 2.81 (d, 2H, $J = 10.7$ Hz, 2 NHCH_2CH), 3.43 (s, 2H, CH_2Ph), 6.98–7.04, 7.23–7.41, 7.64–7.79, and 8.08–8.16 (m, 12H, *aromatics*), 8.48 (t, 1H, $J = 5.0$ Hz, NHCO); 13C-NMR (75,5 MHz, DMSO-d$_6$): 29.9, 35.8, 45.0, 53.1, 62.5, 113.1, 117.2, 119.1, 122.1, 126.5, 126.6, 126.8, 128.1, 128.7, 131.8, 138.8, 154.0, 158.2, 166.6. ESI-MS (positive, *m/z*): 441 (M + 1), 880 (2M + 1); HPLC-HRMS: t_R=5.00 min, calculated 456.2394 found 456.2375. HPLC-HRMS: t_R=4.84 min, calculated 441.2285, found 441.2266.

4.3.14. N-(2-(4-benzylpiperazin-1-yl)ethyl)-2-(2-hydroxyphenyl)-1H-benzo[d]imidazole-5-carboxamide (2)

Starting from 2-(2-hydroxyphenyl)-1H-benzo[d]imidazole-5-carboxylic acid (**8**) (254 mg) and 2-(4-benzyl-1-piperazinyl)ethanamine (**12**) (220 mg), eluent: DCM/MeOH 95:5, the title compound was obtained as a yellow solid, yield =21%; m.p.=249–252 °C. ^{1}H NMR (400 MHz, DMSO-d$_6$), δ (ppm): 2.34–2.47 (m, 10H, 8 piperazine and 2 NH$_2$–CH$_2$CH_2N), 3.36–3.41 (m, 4H, 2 NCH_2Ph and 2 NH$_2$–CH_2CH$_2$N), 6.99–7.40, 7.66–7.79, and 8.07–8.14 (m, 12H, aromatics), 8.41 (t, 1H, $J = 5.3$ Hz, NHCO). 13C-NMR (100.5 MHz, DMSO-d$_6$), δ (ppm): 37.0, 52.7, 52.9, 57.1, 62.2, 112.5, 117.3, 119.3, 122.4, 126.6, 126.9, 128.2, 128.6, 129.4, 132.2, 138.3, 153.3, 158.1, 166.4. ESI-MS (positive, *m/z*): 456 (M + 1); HPLC-HRMS: t_R=5.00 min, calculated 456.2394, found 456.2375.

4.3.15. N-(2-(4-benzylpiperazin-1-yl)ethyl)-7-hydroxybenzofuran-2-carboxamide (3)

Starting from 7-hydroxybenzofuran-2-carboxylic acid (**11**) (178 mg) and 2-(4-benzyl-1-piperazinyl)ethanamine (**12**) (220 mg), eluent: DCM/MeOH 95:5, then acetonitrile/water 19:1, afforded the title product as a white solid, yield =14.2%, m.p.=84–85 °C; ^{1}H NMR (300 MHz, DMSO-d$_6$), δ (ppm): 2.08–2.50 (m, 10H, 8 *piperazine* and CON–CH$_2$CH_2), 3.17–3.44 (m, 2H, CON–CH_2CH$_2$), 3.49 (s, 2H, NCH_2Ph), 6.85–6.97 (m, ^{1}H, *Ph*benzofuran), 7.05–7.12 (m, 2H, *Ph*benzofuran), 7.23–7.34 (m, 5H, CH$_2$*Ph*), 7.42 (s, 1H, benzofuran), 8.41 (t, 1H, $J = 5.3$ Hz, NHCO); 13C-NMR (75.5 MHz, DMSO-d$_6$), δ (ppm): 36.3, 52.6, 52.8, 56.9, 62.1, 109.7, 112.2, 112.4, 124.4, 126.9, 128.2, 128.9, 129.0, 138.3, 143.8, 143.8, 148.8, 158.2. ESI-MS (positive, *m/z*): 380 (M + 1); HPLC-HRMS: $t_R = 4.76$ min, calculated 380.1962, found 380.1930.

4.3.16. General method for synthesis of the compounds 4–7 (method B)

A mixture of benzofuran-2-carboxylic acid (**9**) or 7-methoxybenzofuran-2-carboxylic acid (**10**) (1 eq), NMM (294 mg, 2.5 eq), and T3P (477 mg, 1.5 eq) was stirred in anhydrous DCM under N_2 atmosphere. After 30 min, the amine derivatives 2-(4-benzyl-1-piperazinyl)ethanamine (**12**) or (1-benzylpiperidin-4-yl)methanamine (**13**) (1 eq) were added and the reaction mixture was stirred at RT overnight. To the resulting solution was then added water and ethyl acetate, and extracted. The aqueous layer was extracted with ethyl acetate (3 times), and the organic layers were combined, washed with 1 N NaOH (3 times) and brine (3 times), dried over anhydrous sodium sulphate, and then concentrated under reduced pressure. The crude was purified by column chromatography (eluent: DCM/MeOH 98:2 for compounds **4**, **6**; 92:8 for compounds **5**, **7**) affording the title compounds.

4.3.17. N-((1-benzylpiperidin-4-yl)methyl)benzofuran-2-carboxamide (4)

Starting from benzofuran-2-carboxylic acid (**9**) (162 mg) and (1-benzylpiperidin-4-yl)methanamine (**13**) (204 mg), the title compound was obtained as a white solid, yield =30.5%; m.p.=91–93 °C. ^{1}H NMR (300 MHz, DMSO-d$_6$), δ (ppm): 1.16–1.23, 1.61–1.65, 1.84–1.91 and 3.14–3.18 (m, 9H, *piperidine*), 2.78 (d, 2H, $J = 11.1$ Hz, CH_2CH), 3.42 (s, 2H, NCH_2Ph), 7.22–7.77 (m, 10H, *aromatics*), 8.73 (t, 1H, $J = 5.7$ Hz, N*H*CO); 13C NMR (75.5 MHz, CDCl$_3$), δ (ppm): 29.8, 36.0, 44.8, 53.2, 63.2, 110.4, 111.8, 122.8, 123.8, 126.9, 127.3, 127.7, 128.3, 129.4, 137.6, 148.8, 154.8, 159.1. *m/z*, ESI-MS (positive, *m/z*): 349 (M + 1); HPLC-HRMS: t_R=4.94 min, calculated 349.1911, found 349.1897.

4.3.18 N-(2-(4-benzylpiperazin-1-yl)ethyl)benzofuran-2-carboxamide (5)

Starting from benzofuran-2-carboxylic acid (**9**) (162 mg) and 2-(4-benzyl-1-piperazinyl)ethanamine (**12**) (220 mg), the title compound was obtained as a white solid, yield =40%; m.p.=89–91 °C; ^{1}H NMR (400 MHz, CDCl$_3$), δ (ppm): 2.38–2.52 (m, 8H, *piperazine*), 2.56 (t, 2H, $J = 6.0$ Hz, NH$_2$–CH$_2$CH_2N), 3.47 (s, 2H, NCH_2Ph), 3.50–3.53 (m, 2H, NH$_2$–CH_2CH$_2$N), 7.15–7.45 and 7.58–7.60 (m, 10H, *aromatics*); ^{13}C NMR (100.5 MHz, CDCl$_3$), δ (ppm): 36.0, 53.0, 53.1, 56.5, 63.1, 110.3, 111.9, 122.8, 123.7, 126.8, 127.2, 127.8, 128.4, 129.3, 138.1, 149.0, 154.9, 159.0. ESI-MS (positive, *m/z*): 364 (M + 1), 386 (M + Na); HPLC-HRMS: t_R=4.97 min, calculated 364.2020, found 364.2003.

4.3.19 N-((1-benzylpiperidin-4-yl)methyl)-7-methoxy-benzofuran-2-carboxamide (6)

Starting from 7-metoxy-benzofuran-2-carboxylic acid (**10**) (192 mg) and (1-benzylpiperidin-4-yl)methanamine (**13**) (204 mg), the title compound was obtained as a colourless oil, yield =26%. ^{1}H NMR (300 MHz, DMSO-d$_6$), δ (ppm): 1.06–1.23, 1.55–1.64, 1.84–1.91 and

3.13–3.17 (m, 9H, *piperidine*), 2.78 (d, 2H, $J = 10.9$ Hz, CH_2CH), 3.42 (s, 2H, NCH_2Ph), 3.95 (s, 3H, CH_3O), 7.04–7.06 and 7.21–7.49 (m, 9H, *aromatics*), 8.67 (t, 1H, $J = 5.6$ Hz, N*H*CO); ^{13}C NMR (75.5 MHz, DMSO-d_6), δ (ppm): 29.7, 30.6, 35.6, 44.2, 52.9, 55.8, 62.3, 62.9, 108.6, 109.42 111.2, 114.3, 124.3, 126.3, 126.7, 128.0, 128.6, 138.6, 143.5, 145.2, 149.3, 158.0. ESI-MS (positive, *m/z*): 379 (M + 1); HPLC-HRMS: t_R=5.04 min, calculated 379.2016, found 379.2032.

4.3.20. N-(2-(4-benzylpiperazin-1-yl)ethyl)-7-methoxybenzofuran-2-carboxamide (7)

Starting from 7-methoxybenzofuran-2-carboxylic acid (192 mg, **10**) and 2-(4-benzyl-1-piperazinyl)ethanamine (**12**) (220 mg), the title compound was obtained as a yellow oil, yield =52%; ^1H NMR (300 MHz, $CDCl_3$), δ (ppm): 2.57–3.21 (bs, 10H, 8 *piperazine* + CH_2CH_2N), 3.72 (bs, 2H, CH_2NHCO), 3.80 (s, 2H, NCH_2Ph), 4.05 (s, 3H, CH_3O), 6.88–6.98 and 7.17–7.73 (m, 9H, *aromatics*); ^{13}C NMR (75.5 MHz, $CDCl_3$), δ (ppm): 35.6, 51.4, 51.8, 56.3, 56.8, 62.0, 108.7, 111.0, 114.9, 124.5, 127.1, 127.7, 128.5, 128.7, 128.8, 129.3, 130.1, 144.5, 145.7, 148.7, 159.2. ESI-MS (positive, *m/z*): 394 (M + 1); HPLC-HRMS: t_R=4.97 min, calculated 394.2125, found 394.2121.

4.4 Inhibition of AChE

An adaptation of the Elmman method, previously described, was used to measure the AChE inhibitory activity[31,39]. The assay solution contained 374 µl of (4-(2-hydroxyethyl)-1-piperazineethanesulfonic acid (Hepes) buffer (50 mM and pH 8.0), 476 µl of 5,5′-dithiobis-(2-nitrobenzoic acid) (DTNB, 3 mM), a variable volume (10–50 µl) of the stock solution of each compound in methanol (1 mg/ml), 25 µl of AChE (type VI-S, from electric eel) stock solution and the necessary amount of methanol to obtain 0.925 ml of sample mixture in a 1 ml cuvette. The samples were incubated for 15 min and then 75 µl of acetylthiocholine iodide (AChI) solution (16 mM) was added. The reaction was monitored for 5 min at 405 nm. Assays were run with a blank containing all the components except AChE, which was replaced by Hepes buffer. The velocities of the reaction were calculated as well as the enzyme activity. A control reaction was carried out using methanol as a sample solution and it was considered as 100% activity. The percentage inhibition of the enzyme activity due to the presence of increasing test compound concentration was calculated by the following Eq. (1),

$$\%I = 100 - 100 \times v_i/(v_i - v_o), \quad (1)$$

v_i starting reaction rate in the presence of inhibitor, v_o starting rate of the control reaction.

The inhibition curves were obtained by plotting the percentage of enzymatic inhibition versus inhibitor concentration and a calibration curve was obtained from which the linear regression parameters were obtained.

4.5 Anti-oxidant activity

The antioxidant activity (free radical scavenging activity) was evaluated by DPPH (2,2-diphenyl-1-picrylhydrazyl) assay, as previously described in literature[31,39]. To a 2.5 ml solution of DPPH (0.002%) in methanol, five samples of each compound solution were added with different volumes of methanol in order to obtain five different concentrations in a 3.5 ml final volume. The samples were incubated for 30 min at RT and protected from the light. The absorbance was measured at 517 nm using pure methanol as a blank sample. The antioxidant activity was calculated by the Eq. (2).

$$\%AA = 100 \times (A_{DPPH} - A_{sol})/A_{DPPH} \quad (2)$$

The tests were carried out in duplicate. The compound's concentration providing 50% of antioxidant activity (EC_{50}) was obtained by plotting the antioxidant activity against the compound's concentration.

4.6 Inhibition of self- and Cu(II)-mediated $A\beta_{1-42}$ aggregation

The samples were treated with 1,1,1,3,3,3-hexafluoropropan-2-ol (HFIP) and dissolved in a CH_3CN/Na_2CO_3 (300 µM)/NaOH (250 µM) (48.3:48.3:4.3,v/v/v) solvent mixture in order to have a stable stock solution, avoiding self-aggregation of $A\beta_{1-42}$. Then, the 500 µM solution was diluted at 40 µM in phosphate buffer (0.215 M, pH 8.0).

The tested compounds were diluted in MeOH (1 mg/ml), being further diluted in phosphate buffer to a concentration of 480 µM. For copper-induced aggregation studies was used a solution of $CuCl_2$ 240 µM, prepared from a stock solution (0.015 M). To study the $A\beta_{1-42}$ aggregation inhibition, a reported method, based on the fluorescence emission of thioflavin T (ThT), was followed[16,48,49]. $A\beta_{1-42}$ (40 µM) was incubated at 37 °C, for 24 h with or without Cu(II) (40 µM) in a phosphate buffer in presence or absence of the single ligand (80 µM). Then, the samples were added to a 96-well plate with 180 µM of 5 µM ThT in 50 mM glycine–NaOH (pH 8.5) buffer. Blank samples were prepared without the peptide for each concentration. The ThT fluorescence was measured at 446 nm (excitation) and 485 nm (emission). The inhibition percentage of aggregation was calculated by Eq. (3), in which IF_i and IF_0 corresponded to the fluorescence intensities, in the presence and the absence of the tested compound, subtracted of the fluorescence intensities due to the respective blanks.

$$I\% = 100 - (IF_i/IF_0 \times 100) \quad (3)$$

The reported values were obtained as the mean ± SEM of duplicate of two different experiments.

For the preparation of the TEM samples, a film of $A\beta_{1-42}$ was dissolved in a fresh mixture of 106.6 µl of CH_3CN/NaCl (300 µM)/NH_4OH (2%) (48.3/48.3/10.0 µl v/v/v) by brief sonication. To the resulting alkaline $A\beta_{1-42}$ solution (346.35 µM) was added 631.80 µl of HEPES buffer 50 mM, pH 6.6, affording a concentration of $A\beta_{1-42}$ of 50 µM. The compounds tested were diluted in MeOH (1 mg/ml), being further diluted in HEPES buffer to a concentration of 240 µM. For copper-induced aggregation studies was used a solution of $CuCl_2$ 120 µM. Blank or treated samples at 50 µM, in presence or absence of Cu^{2+}, were added to the solution of Aβ, obtaining 25 µM as final concentration. Then, the sample was incubated in a water bath CERTOMAT WR for 24 h at 37 °C with gentle shaking.

Formvar/carbon 200-mesh Cu grids (Ted Pella) were treated with Aβ peptide aggregated samples (10 µl) for 2 min at RT. Excess samples were removed using filter paper followed by washing twice with deionised water. Each grid incubated with uranyl acetate (1%, 10 µl, 1 min) was stained and dried for 15 min at RT.

4.7. Cell viability and neuroprotection

SH-SY5Y human neuroblastoma cell line (ATCC-CRL-2266) grown in Dulbecco's modified Eagle's medium (DMEM) obtained from

Gibco-Invitrogen (Life Technologies Ltd, UK) with 10% heat inactivated fetal calf serum, containing 50 U/ml penicillin, and 50 μg/ml streptomycin, under a humidified atmosphere of 95% air–5% CO_2 at 37 °C. Cells were plated at 0.12×10^6 cells/ml for cell viability assay. The tested compounds (**1, 2, 4, 5** and **7**) were dissolved in DMSO at a concentration of 25 mM and aliquots were stored at –20 °C. We performed a concentration screening (from 5 to 30 μM) in order to choose the highest nontoxic concentration. As a result compound **1** was added to the medium at 2.5 μM final concentration; compound **2** was added to the medium at 5 μM final concentration; compounds **4**, **5** and **7** were added to the medium at 30 μM final concentration; and compound **6** was added to the medium at 20 μM final concentration. The final concentration of DMSO in culture media did not exceed 0.05% (v/v) and no alterations on cells were observed. Cells were pre-incubated for 1 h with the compounds and then incubated with $A\beta_{1-42}$ for an additional 24 h. $A\beta_{1-42}$ was prepared as 276.9 μM stock in sterile water and added to the medium at 1 μM final concentration. $A\beta_{1-42}$ was purchased from Bachem (Torrance, CA, USA). For all conditions tested, control experiments were performed in which the compounds tested, $A\beta_{1-42}$ was not added.

Cell viability was determined by the colorimetric MTT (3-(4,5-dimethylthiazol-2-yl)-2,5-diphenyltetrazolium bromide) assay[50]. In viable cells, the enzyme succinate dehydrogenase metabolises MTT into a formazan that absorbs light at 570 nm. Following the cell treatment protocol the medium was aspirated and 0.5 ml MTT (0.5 mg/ml) was added to each well. The plate was then incubated at 37 °C for 3 h. At the end of the incubation period the formazan precipitates were solubilised with 0.5 ml of acidic isopropanol (0.04 M HCl/isopropanol). The absorbance was measured at 570 nm. Cell reduction ability was expressed as a percentage of untreated control cells.

All data were expressed as mean ± SEM of at least three independent experiments performed in duplicates. Statistical analyses were performed using one-way ANOVA followed by Bonferroni multiple comparisons procedure *post hoc* test. A p value <0.05 was considered statistically significant.

4.8 Prediction of pharmacokinetic properties

To analyze the potential of the new compounds as new drugs active in CNS, a prediction on pharmacokinetic properties was calculated *in silico*. Parameters such as the octanol-water partition coefficient (clog *P*), BBB partition coefficient (log BB), the ability to be absorbed through the intestinal tract (Caco-2 cell permeability) and CNS activity were calculated. The chemical structures were minimised as previously described for the docking studies and they were submitted to the calculation of these relevant pharmacokinetic proprieties and descriptors using QikProp v. 2.5[40].

Acknowledgements

The authors thank the financial support to the Portuguese Fundação para a Ciência e Tecnologia (FCT) for the projects UID/QUI/00100/2013 and PEst-C/SAU/LA0001/2011–2013. Acknowledgements are also due to the Portuguese NMR (IST-UL Center) and Mass Spectrometry Networks (Node IST-CTN) for providing access to their facilities. The authors acknowledge also Dr. Lucia Gambacorta and CNR-ISPA (Bari, Italy) for HPLC-HRMS analyses. L.P. thanks Fondo di Sviluppo e Coesione 2007–2013–APQ Ricerca Regione Puglia "Programma regionale a sostegno della specializzazione intelligente e della sostenibilità sociale ed ambientale - Future In Research". Project ID: I2PCTF6.

Disclosure statement

No potential conflict of interest was reported by the authors.

ORCID

Luca Piemontese http://orcid.org/0000-0002-7980-5818
Daniel Tomás http://orcid.org/0000-0002-9000-0535
Asha Hiremathad http://orcid.org/0000-0001-7170-2614
Vito Capriati http://orcid.org/0000-0003-4883-7128
Emanuel Candeias http://orcid.org/0000-0002-8511-5821
Sandra M. Cardoso http://orcid.org/0000-0002-2199-0555
Sílvia Chaves http://orcid.org/0000-0002-8554-4992
M. Amélia Santos http://orcid.org/0000-0002-4069-9368

References

1. a) Alzheimer's Association. Alzheimer's disease facts and figures. Alzheimers Dement 2017;13:325–73. b) World Health Organization. Dementia, WHO fact sheet: 2017; http://www.who.int/mediacentre/factsheets/fs362/en/
2. a) Grill JD, Cummings JL. Current therapeutic targets for the treatment of Alzheimer's disease. Expert Rev Neurother 2010;10:711–28. b) Cummings JL, Morstorf T, Zhong K. Alzheimer's disease drug-development pipeline: few candidates, frequent failures. Alzheimers Res Ther 2014;6:37.
3. Querfurth HW, LaFerla FM. Alzheimer's disease. N Engl J Med 2010;362:329–44.
4. Santos MA, Chand K, Chaves S. Recent progress in repositioning Alzheimer's disease drugs based on a multitarget strategy. Future Med Chem 2016;8:2113–42.
5. a) Ghosh AK, Osswald HL. BACE1 (β-secretase) inhibitors for the treatment of Alzheimer's disease. Chem Soc Rev 2014;43:6765–813. b) Zheng H, Amit T, Bar-Am O, et al. From anti-Parkinson's drug rasagiline to novel multitarget iron chelators with acetylcholinesterase and monoamine oxidase inhibitory and neuroprotective properties for Alzheimer's disease. Alzheimer's Dis 2012;30:1–16.
6. a) Parsons CG, Stöffler A, Danysz W. Memantine: a NMDA receptor antagonist that improves memory by restoration of homeostasis in the glutamatergic system—too little activation is bad, too much is even worse. Neuropharmacol 2007;53:699–723. b) Bernardo A, Minghetti L. PPAR-gamma agonists as regulators of microglial activation and brain inflammation. Cur Pharm Des 2006;12:93–109. c) Piemontese L. New approaches for prevention and treatment of Alzheimer's disease: a fascinating challenge. Neur Reg Res 2017;12:405–6.
7. Ansari MA, Scheff SW. Oxidative stress in the progression of Alzheimer disease in the frontal cortex. J Neuropathol Exp Neurol 2010;69:155–67.
8. Bush AI, Tanzi RE. Therapeutics for Alzheimer's disease based on the metal hypothesis. Neurotherapeutics 2008;5:421–32.

9. Santos MA, Chand K, Chaves S. Recent progress in multifunctional metal chelators as potential drugs for Alzheimer's disease. Coord Chem Rev 2016;327–328:287–303.
10. a) Hiremathad A. A review: natural compounds as anti-Alzheimer's Disease agents. Curr. Food Nutr. Sci 2017;13:247254. b) Piemontese L. Plant food supplements with antioxidant properties for the treatment of chronic and neurodegenerative diseases: benefits or risks? J Diet Suppl 2017;14:478–84.
11. Zemek F, Drtinova L, Nepovimova E, et al. Outcomes of Alzheimer's disease therapy with acetylcholinesterase inhibitors and memantine. Expert Opin Drug Saf 2014;13:759–74.
12. Cavalli A, Bolognesi ML, Minarini A, et al. Multi-target-directed ligands to combat neurodegenerative diseases. J Med Chem 2008;51:2326–72.
13. Guzior N, Ckowska AW, Panek D, Malawska B. Recent development of multifunctional agents as potential drug candidates for the treatment of Alzheimer's disease. Curr Med Chem 2015;22:373–404.
14. Unzeta M, Esteban G, Bolea I, et al. Multi-Target directed donepezil-like ligands for Alzheimer's disease. Front Neurosci 2016;10:205.
15. Benek O, Soukup O, Pasdiorova M, et al. Design, synthesis and in vitro evaluation of indolotacrine analogues as multi-target-directed ligands for the treatment of Alzheimer's disease. ChemMedChem 2016;11:1264–9.
16. Hiremathad A, Chand K, Esteves AR, et al. Tacrine-allyl/propargylcysteine-benzothiazole trihybrids as potential anti-Alzheimer's drug candidates. RSC Adv 2016;6:53519–32.
17. Spilovska K, Korabecny J, Nepovimova E, et al. Multitarget tacrine hybrids with neuroprotective properties to confront Alzheimer's disease. Curr Top Med Chem 2017;17:1006–26.
18. Prati F, Bergamini C, Fato R, et al. Novel 8-hydroxyquinoline derivatives as multitarget compounds for the treatment of Alzheimer's disease. ChemMedChem 2016;11:1284–95.
19. Hiremathad A, Keri RS, Esteves AR, et al. Novel tacrine-hydroxyphenylbenzimidazole hybrids as potential multitarget drug candidates for Alzheimer's disease. Eur J Med Chem 2018;148:255–67.
20. Panek D, Więckowska A, Wichur T, et al. Design, synthesis and biological evaluation of new phthalimide and saccharin derivatives with alicyclic amines targeting cholinesterases, beta-secretase and amyloid beta aggregation. Eur J Med Chem 2017;125:676–95.
21. Mezeiova E, Spilovska K, Nepovimova E, et al. Profiling donepezil template into multipotent hybrids with antioxidant properties. J Enzyme Inhib Med Chem 2018;33:583–606.
22. Hiremathad A, Piemontese L. Heterocyclic compounds as key structures for the interaction with old and new targets in Alzheimer's disease therapy. Neural Regen Res 2017;12:1256–61.
23. Keri RS, Hiremathad A, Budagumpi S, Nagaraja BM. Comprehensive review in current developments of benzimidazole-based medicinal chemistry. Chem Biol Drug Des 2015;86:19–65.
24. Chand K, Rajeshwari, Hiremathad A, et al. A review on antioxidant potential of bioactive heterocycle benzofuran: natural and synthetic derivatives. Pharmacol Rep 2017;69:281–95.
25. Coban G, Carlino L, Tarikogullari AH, et al. 1H-benzimidazole derivatives as butyrylcholinesterase inhibitors: synthesis and molecular modeling studies. Med Chem Res 2016;25:2005–14.
26. Hiremathad A, Chand K, Tolayan L, et al. Hydroxypyridinone-benzofuran hybrids with potential protective roles for Alzheimer's disease therapy. J Inorg Biochem 2018;179:82–96.
27. Korabecny J, Dolezal R, Cabelova P, et al. 7-MEOTA-donepezil like compounds as cholinesterase inhibitors: synthesis, pharmacological evaluation, molecular modeling and QSAR studies. Eur J Med Chem 2014;82:426–38.
28. a) Kryger G, Silman I, Sussman JL. Structure of acetylcholinesterase complexed with E2020 (Aricept): implications for the design of new anti-Alzheimer drugs. Structure 1999;7:297–307. b) Kryger G, Silman I, Sussman JL. The peripheral anionic site of acetylcholinesterase: structure, functions and potential role in rational drug design. Curr Pharm Des 1999;7:297–25.
29. Cheung J, Rudolph MJ, Burshteyn F, et al. Structures of human acetylcholinesterase in complex with pharmacologically important ligands. J Med Chem 2012;55:10282–6.
30. Karthikeyan C, Solomon VR, Lee H, Trivedi P. Synthesis and biological evaluation of 2-(phenyl)-3H-benzo[d]imidazole-5-carboxylic acids and its methyl esters as potent anti-breast cancer agents. Arab J Chem 2017;10:S1788–S94.
31. Quintanova C, Keri RS, Marques SM, et al. Design, synthesis and bioevaluation of tacrine hybrids with cinnamate and cinnamylidene acetate derivatives as potential anti-Alzheimer drugs. MedChemComm 2015;6:1969–77.
32. Zagidullin RN. Reactions of *N*-(β-aminoethyl)piperazine and its derivatives. Chem Heterocycl Comp 1991;27:309–12.
33. Porcelli L, Gilardi F, Laghezza A, et al. Synthesis, characterization and biological evaluation of ureidofibrate-like derivatives endowed with peroxisome proliferator-activated receptor activity. J Med Chem 2012;55:37–54.
34. Chaves S, Hiremathad A, Tomás D, et al. Exploring the chelating capacity of 2-hydroxyphenylbenzimidazole based hybrids with multi-target ability as anti-Alzheimer's agents [unpublished results]
35. Faller P, Hureau C, La Penna G. Metal ions and intrinsically disordered proteins and peptides: from Cu/Zn amyloid-β to general principles. Acc Chem Res 2014;47:2252–9.
36. Fancellu G, MSc Thesis. Pisa: University of Pisa; 2018.
37. Tepe B, Daferera D, Sokmen A, et al. Antimicrobial and antioxidant activities of the essential oil and various extracts of *Salvia tomentosa Miller* (Lamiaceae). J Agric Food Chem 2005;90:333–40.
38. Valko M, Rhodes CJ, Moncol J, et al. Free radicals, metals and antioxidants in oxidative stress-induced cancer. Chem Biol Interact 2006;160:1–40.
39. Šebestík J, Marques SM, Falé PL, et al. Bifunctional phenolic-choline conjugates as anti-oxidants and acetylcholinesterase inhibitors. J Enzyme Inhib Med Chem 2011;26:485–97.
40. Schrödinger L. QikProp version 2.5. New York, NY: Schrödinger, LLC; 2005.
41. Lipinski CA, Lombardo F, Dominy BW, Feeney PJ. Experimental and computational approaches to estimate solubility and permeability in drug discovery and development settings. Adv Drug Deliv Rev 2012;64:4–17.
42. Armarego WLF, Perring DD, Purification of laboratory chemicals, 4th ed. Oxford: Butterworth–Heinemann Press; 1999.
43. Keri RS, Quintanova C, Marques SM, et al. Design, synthesis and neuroprotective evaluation of novel tacrine-benzothiazole hybrids as multi-targeted compounds against Alzheimer's disease. Bioorg Med Chem 2013;21:4559–69.
44. Maestro version 9.3. Portland, OR: Schrödinger Inc.; 2012.
45. Hassinen T, Peräkylä M. New energy terms for reduced protein models implemented in an off-lattice force field. J Comput Chem 2001;22:1229–42.
46. Acton A, Banck M, Bréfort J, et al. Ghemical version 3.0 2011.

47. Jones G, Willett P, Glen RC, et al. Development and validation of a genetic algorithm for flexible docking. J Mol Biol 1997;267:727–48.
48. Bartolini M, Bertucci C, Bolognesi ML, et al. Insight into the kinetic of amyloid beta (1–42) peptide self-aggregation: elucidation of inhibitors' mechanism of action. ChemBioChem 2007;8:2152–61.
49. Chao X, He X, Yang Y, et al. Design, synthesis and pharmacological evaluation of novel tacrine-caffeic acid hybrids as multi-targeted compounds against Alzheimer's disease. Bioorg Med Chem Lett 2012;22:6498–502.
50. Mosmann T. Rapid colorimetric assay for cellular growth and survival: application to proliferation and cytotoxicity assays. J Immunol Methods 1983;65:55–63.